Available online at www.sciencedirect.com
SCIENCE DIRECT
NDT&E International 38 (2005) 634–642
NDT&E international
www.elsevier.com/locate/ndteint

A focused two-dimensional air-coupled ultrasonic array for non-contact generation

Frank Blum[a,1], Jacek Jarzynski[b], Laurence J. Jacobs[a,b,*]

[a]School of Civil and Environmental Engineering, Georgia Institute of Technology, Atlanta, GA 30332-0355, USA
[b]G.W. Woodruff School of Mechanical Engineering, Georgia Institute of Technology, Atlanta, GA 30332-0405, USA

Received 3 September 2004; revised 10 March 2005; accepted 11 March 2005
Available online 29 April 2005

Abstract

Air-coupled ultrasonic sources are relatively inefficient because the high impedance mismatch at the air/solid boundary means that most of the input energy (in air) is reflected at this boundary. The objective of this research is to increase efficiency—specifically an increase in ultrasonic signal amplitude—by designing and building a focused, 2D-array of electrostatic transducers (individual diameters of 38 mm). The operating frequency of this array is in the range of 50–100 kHz; this range is selected for civil infrastructure applications. Numerical simulations are used to design an array by modeling the pressure field in air, and then optimizing an array consisting of 20 transducers to create a line-source. An array is then built (following this design) and the emitted pressure field (in air) of the as built array is measured with a microphone and compared to the pressure field predicted by the numerical model. Finally, the as built focused array is used as an ultrasonic source, and its robustness is verified by comparing the numerical simulation of a transient line-load on an elastic half-space with (completely non-contact) experimentally measured values. There is excellent agreement between these two representations, which confirms the possibility of developing a completely non-contact, scanning ultrasonic system in the 50–100 kHz range.

Keywords: Air-coupled ultrasound; Generation; Focused array

1. Introduction

There is a significant need for reliable and accurate non-destructive evaluation (NDE) techniques to examine civil infrastructure, such as concrete components. Critical requirements of any candidate NDE system for civil infrastructure is the ability to quickly interrogate large-scale structural components, while providing quantitative information about the structural health of that component.

Previous researchers [1] have summarized potential NDE methods for testing concrete components that do not use acoustic waves—radiography, infrared thermography, and microwave-B-scan. Popular ultrasonic techniques for concrete components include the pulse-velocity and pulse-echo techniques, where time-of-flight and amplitude measurements can be used to determine the existence of any internal defects, measure material stiffness [2], or make tomographic images [3]. Pulse-echo is a single sided technique (of practical importance when access is only available to one side of a component) that has shown great promise for concrete structures [4]. The frequency range of ultrasonic waves typically used to interrogate concrete components is in the 25–250 kHz range [4,5].

Unfortunately, the applicability of these elastic wave based methodologies for field measurements is limited because conventional ultrasonic testing uses transducers that must be in direct contact with a component, or must use a coupling medium such as water. There are completely non-contact ultrasonic methods—including laser based and air-coupled ultrasonic techniques—so it is possible to design a scanning system to interrogate large structural components. The non-contact detection of ultrasound can be accomplished with optical techniques such as a laser Doppler vibrometer (LDV) [6,7], while non-contact generation of ultrasound can be achieved with a pulsed laser [8].

* Corresponding author. Address: School of Civil and Environmental Engineering, Georgia Institute of Technology, Atlanta, GA 30332-0355, USA. Tel.: +1 404 894 2771; fax: +1 404 894 2278.
E-mail address: laurence.jacobs@ce.gatech.edu (L.J. Jacobs).
[1] Present address: Institute A for Mechanics, University of Stuttgart, Stuttgart, Germany.

0963-8695/$ - see front matter © 2005 Elsevier Ltd. All rights reserved.
doi:10.1016/j.ndteint.2005.03.002

However, the amplitude and frequency content of ultrasonic waves generated with a pulse laser are not ideal for the in situ interrogation of large concrete components—the amplitudes are relatively low, while the frequency content is relatively high (in the low mega-hertz range) [9]. A candidate non-contact, ultrasonic source for civil infrastructure applications is an air-coupled, ultrasonic transducer operating in the frequency range of 50–100 kHz.

The air-coupled generation of ultrasound is truly non-contact, but has the disadvantage of low signal amplitude—the high impedance mismatch at the air/solid boundary means that most of the input energy (in air) is reflected at this boundary. One way to increase signal amplitude is to combine several air-coupled ultrasonic transducers into an array. The objective of this research is to increase efficiency—defined as an increase in ultrasonic signal amplitude—by designing and building a focused, two-dimensional array (2D-array) of electrostatic transducers (commercially available, individual diameters of 38 mm). The operating frequency of this array is in the range from 50 to 100 kHz. Note, that this design is in contrast to small scale arrays [10,11] and focused parabolic mirrors [12] which are designed to operate in the mega-hertz frequency range. Previous research has used a single air-coupled transducer for non-contact generation of ultrasound in civil infrastructure, such as railroad rails [13].

An extensive review of the work on contactless, air-coupled ultrasonic systems prior to 1995 is presented in [14]. Much of the previous work is aimed at development of contactless systems for non-destructive evaluation (NDE) of machinery components and materials in the frequency range from 400 kHz to several MHz. Many of the contactless systems developed use air-coupled transducers both to generate and to receive the ultrasound. A previous study closest to the present work is [15], who used a high-power laser to generate elastic waves in a solid sample and an air-coupled receiving transducer to detect these waves.

This paper describes a procedure to design, build and test a focused aircoupled ultrasonic array. Numerical simulations are used to design an array by modeling the pressure field in air, and then optimizing an array consisting of 20 transducers to create a line-source. The design objective is to position 20 electrostatic transducers in such a way that the signal amplitude at the focal line of the array is maximized. At the end of the design process, a sensitivity study is performed to identify the most critical parameters that change the predicted behavior of the array. An array is then built (following this design) and the emitted pressure field (in air) of the as built array is measured with a microphone, and compared to the pressure field predicted by the numerical model. Finally, the built array is used as an ultrasonic source in a low density polyethylene (LDPE) layer to quantify the ultrasonic signal amplitude and frequency characteristics of the as built array. The robustness of this array source is verified by comparing the numerical simulation of a transient line-load on an elastic half-space with (completely non-contact) experimentally measured values. There is excellent agreement between these two representations, which confirms the efficiency of the as built array, and confirms the possibility of developing a completely non-contact, scanning ultrasonic system in the 50–100 kHz range.

2. Numerical simulation, verification, and optimization

2.1. Single piston source

To model the behavior of a single electrostatic transducer, consider a fluid that contains an acoustic source of a rigid piston of radius, a, mounted flush with the surface of an infinite baffle, and vibrating with a time harmonic motion. Following [16], let the radiating surface of the piston move uniformly with the speed of $U_0 e^{i\omega t}$, normal to the baffle. Note that U_0 is the amplitude of vibration (speed), and ω is the angular frequency. The pressure at any point, (r, θ) in the far field, $r \gg a$, is

$$p(r,\theta,t) = i\frac{\rho_0 c}{2} U_0 \frac{a}{r} ka\, e^{i(\omega t - kr)} \left[\frac{2J_1(ka\sin\theta)}{ka\sin\theta}\right], \quad (1)$$

where c is phase velocity, k is the wavenumber, ρ_0 is mass density of an undisturbed fluid element, and J_1 is the Bessel-function of the first kind of order one. The angular dependence of p is contained in the bracketed term, and this term goes to unity as θ goes to zero. This angular dependency is a function of ka, and yields the directivity pattern of the circular piston. It can be shown that if the radius of the circular piston is large in comparison with the wavelength, λ, of sound ($ka \gg 1$), the directivity pattern has many side-lobes and the angular width of the main-lobe is small. On the other hand, if the wavelength is much greater than the radius ($ka \ll 1$), only the main-lobe will be present, see [16] or [17] for detailed plots. Note that the derivation of Eq. (1) assumes that the piston is mounted on an ideal infinite baffle. This model corresponds quite closely to the measured pressure pattern of piston-type loudspeakers for high frequencies, even if the baffle is of small linear dimensions [16].

There is significant absorption of sound in air, and its influence must be included in the model. This absorption of sound is expressed as

$$p(x) = p_0 e^{-\alpha x}, \quad (2)$$

where p_0 denotes the pressure without taking absorption into account, x is the propagation distance, and α is the absorption coefficient—proportional to f^2—measured in attenuation per unit length, Np/m. A description of the absorption mechanisms in air, plus an expression for the α used in this study is available in [18].

2.2. Performance of transmitting transducers

The individual elements of the air-coupled array are Polaroid, instrument grade, electrostatic transducers of the 600 Series, which will be referred to as 'transmitting transducers.' These transmitting transducers are specifically intended for operation in air at low ultrasonic frequencies and were originally designed for distance (range) measurements. The moving part of each transmitting transducer is a thin foil which transforms electrical energy into sound waves. This thin foil is made out of Kapton (a plastic) coated with gold on the front side, and is stretched over an aluminum backplate. The thin foil, together with the backplate, represent an electrical capacitor. When an AC voltage is applied to the transmitting transducer, the thin foil is forced to move with the AC frequency of the input signal, and this mechanical motion creates sound waves in air. The specifications of these transmitting transducers (provided by Polaroid [19]) are listed in Table 1.

The variability of eight different transmitting transducers is investigated in order to develop a more statistical representation of transmitting transducer performance. Sound detection in air is accomplished with a G.R.A.S. 40BE pre-polarized free field microphone, a one-quarter inch (6.35 mm) precision microphone for general purpose acoustic measurements at high frequencies and high levels. This microphone is designed to measure the sound pressure as it exists before the microphone is introduced into the sound field, by compensating for any diffraction effects at higher frequencies. The frequency range of this microphone is 2 Hz–100 kHz. The G.R.A.S. microphone is moved along a line parallel to the surface of a transmitting transducer—this line is located at a (perpendicular) distance of 20 cm. The mean values of all eight transmitting transducers (plus standard deviations), along with the pressure field predicted using Eq. (1) is presented in Fig. 1 (driving frequency 80 kHz). There is excellent agreement between the numerically simulated pressure field and the experimentally measured values, and the standard deviations are relatively low. Overall, the numerical simulation predicts the pressure pattern of a single transmitting transducer with a high degree of accuracy, and these results will be used to design an optimized array of 20 transmitting transducers arranged in four rows of five transducers each.

Table 1
Specification of Polaroid 600 Series electrostatic transducers (transmitting transducers) [19]

Active diameter	38 mm
Transmitting frequency range	20–100 kHz
Suggested DC bias voltage	105 V
Suggested AC driving voltage (peak)	150 V
Maximum combined voltage	400 V
Capacitance at 1 kHz	≈400–500 pF

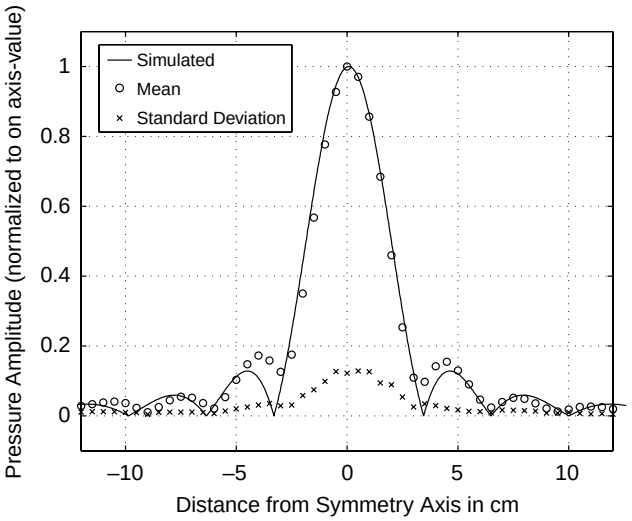

Fig. 1. Mean of eight single transmitting transducers measured at 20 cm.

2.3. Design of the array

This design process uses a genetic optimization algorithm—the principles of a genetic algorithm can be found in [20,21]. The array is designed such that sound pressure amplitude is maximized on a focal line. Fig. 2 shows a sketch of a possible design, where the x, y, and z axes are identified. A single row is designed in a first step, and then

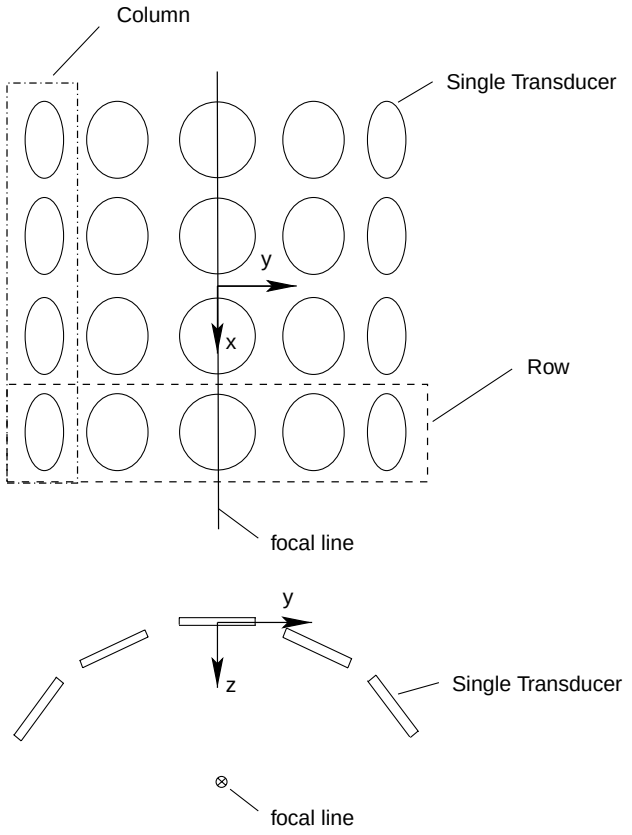

Fig. 2. Schematic of the array.

four of these rows are combined such that the resulting sound pressure along the focal line is at nearly the same level, and in phase.

The design of a single row of transducers optimizes the position and the transmitting direction of the five transmitting transducers for maximum pressure amplitude at the focal line, which will be referred to as the focal point for a single row. In order to restrict the degrees of freedom for this problem, the transmitting transducers are positioned on a circle with radius r symmetrically about the 'symmetry axis'—the axis on which both the middle transmitting transducer and the focal point are located, as shown in Fig. 3. For this case, the five transmitting transducer positions are described in terms of three variables: r, α_1, α_2. The position of the focal point is described by the variable d. The transmission directions are represented by the variables α_3, α_4.

The optimization process is conducted in two steps at a fixed transmitting frequency of 80 kHz. The first step considers the general shape of the array. The six variables (r, d, α_i) are varied within the restrictions due to the size of the transmitting transducers, and the resulting space needed to mount them properly. Two design variants turn out to generate the highest sound pressure amplitude at the focal point. In the first variant, the focal point is located at the center of a circle with a radius of 18 cm. In the second variant, the focal point is located in between the center of a circle (radius 27 cm) and the middle transmitting transducer, with the distance, d, to the focal point of 15 cm.

Comparing these two designs, it is noted that in the first variant, the sound pressure at the focal point is the same even if the angles α_i vary—as long as the transmitting directions are directed towards the center of the circle. This is due to the fact that the focal point is always located on the symmetry axis of each transducer, and the sound pressure amplitude of the transducers reaches its maximum on this axis (as shown in Fig. 1). In contrast, in the second variant, even small variations in α_i have a great influence on the resulting pressure amplitude. Another important issue is the transient behavior of the array since the optimizations so far

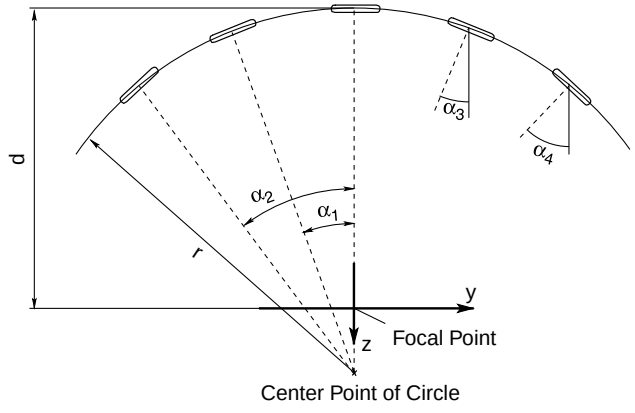

Fig. 3. Schematic of the array parameters adjusted in design optimization.

Table 2
Final design of a single row

Variable	Value
r	20 cm
d	20 cm
α_1 and α_3	16.5°
α_2 and α_4	34°

are performed for the steady-state case of 80 kHz. In the first variant, the propagation distances from all transmitting transducers to the focal point are the same, while in the second variant, these propagation distances are different; the signals from the outer transmitting transducers will reach the focal point later, (and be out of phase) for any transmitting frequency besides 80 kHz with the second variant, therefore the pressure amplitude at the focal point will decrease significantly compared to the first design variant. As a result, the first design variant (focal point at the center of the circle) is selected, and to ensure that the focal point is in the far field at higher frequencies (thus having the pressure pattern shown Fig. 1), a radius, r, of 20 cm is selected.

The parameters α_i can be chosen freely, so the second design objective—that the side-lobes in the y-direction should be small—is now considered. Since there are always going to be large side-lobes (in the y-direction) present, a 'shield plate' with a slit will be used to physically shield (spatially filter out) the largest side-lobes. This shield plate is necessary to ensure that the pressure field at the test object can be realistically treated as a line-source. The use of this shield plate means that it is only important for the design process that the side-lobes near the symmetry axis (where the focal point is located) are small. Note that the width of the slit is selected as an exact multiple of the wavelength (e.g. at 80 kHz, $\lambda = 4.25$ mm) for the best performance [17]. Several optimizations are performed and a design is selected that has small side-lobes near the focal plane, but there is a relatively large side-lobe that is located far enough away from the main lobe that it can be easily shielded out. The parameters of the design ultimately selected for a single row are presented in Table 2.

The second optimization step combines four of these rows—the degree of freedom in this step is the spacing of the rows, and the rows will be equally spaced to ensure a symmetric pattern. The optimization shows that a spacing of 5.08 cm is best with respect to the design objective of smooth (flat) pressure amplitude and phase in the x-direction, while taking the restriction due to the size of the transmitting transducers into account [17].

2.4. Pressure field in the focal plane

Fig. 4 shows the pressure amplitude in the focal plane (x–y plane). The line pattern is clear, and the main-lobe, plus the two major side-lobes are fairly evident. Fig. 5 shows

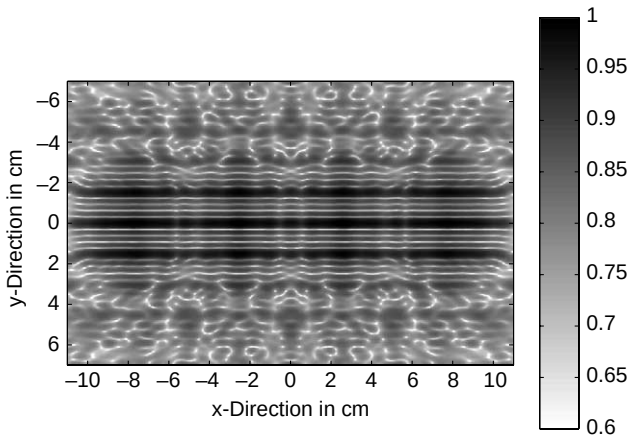

Fig. 4. Pressure amplitude in the focal plane.

the phase in the focal plane. It can be observed that there is a large phase change in the region of the small side-lobes. This phase change is another reason for the shield plate—this plate will shield the pressure contribution of the side-lobes, and thus ensure that the signal at the focal line (the proposed position of the test sample) is in phase, and there are no signal cancellations.

2.5. Sensitivity to detuning

So far, it has been assumed that it is possible to build a perfect array, without any spatial errors. Note that the wavelength of a 80 kHz signal (the transmitting frequency) is $\lambda = 4.25$ mm, so destructive interference can occur if a transmitting transducer is out of position by a few millimeters. In addition, all transmitting transducers do not have exactly the same output pressure amplitude, as shown in Fig. 1. Two sensitivity studies are conducted. The first one examines the sensitivity of the focal line signal to the output-pressure-level of the individual transmitting transducers, while the second one examines the effect of detuning (slightly altering) the spatial position of the individual transmitting transducers.

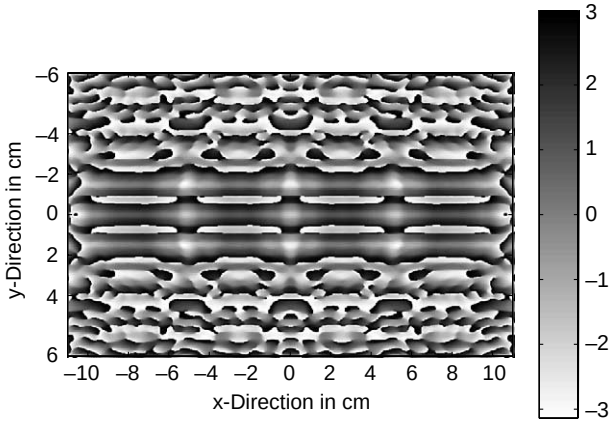

Fig. 5. Pressure phase (radians) in the focal plane.

In order to test the effect of the variation of the output-pressure-level of the individual transmitting transducers, the signal amplitude of the transducers is varied from 70 to 110% in steps of 10% from the outermost left, to the outermost right transducer. This pressure distribution is chosen in order to have an asymmetric sound pressure field, so that the effect on the location of the main-lobe and the side-lobes can be studied. The results of this simulation show that the variation in the output-pressure-level has no effect on the location of the minima and the maxima, and it only effects the height of the main-lobe and the side-lobes. The main-lobe, as well as the largest side-lobe are decreased by approximately 10%, while the first side-lobe is increased by 10% in signal strength. This behavior is not critical for the design of the array, since the changes in the signal amplitude are acceptable, and the shape of the sound field does not change.

Next, seven tests are conducted to examine how variations in transmitting transducer position influences the pressure pattern at the focal line. These variations in transmitting transducer position could be due to machining errors, or positioning inaccuracy. The results show that moving a transmitting transducer radially towards the focal line has the most significant effect on the resulting pressure pattern of the focal line, while changes tangential to the circle have only minor effects on the pattern. Changes in the transmitting direction has relatively insignificant influence on the pressure pattern of the focal line. For example, when two transducers are moved 1 mm in the negative z-direction, the pressure amplitude of the main-lobe drops by 25% compared to the optimum configuration.

3. Performance of the as built array

3.1. Sound field emitted in air

The performance of the actual array—which will be referred to as the ‘as built’ array—is quantified by measuring the pressure amplitude along the y- and x-axes; these results are compared to the numerically predicted values, and then the absolute value of the sound pressure at the focal line is measured. Proper alignment of the as built array plays a critical role in array performance. Therefore, metal shims are used to get the signals of the individual transmitting transducers in phase at the focal line. The actual pressure amplitude emitted by a row of this ‘aligned’ as built array is measured along the y-axis with the G.R.A.S. microphone, and presented in Fig. 6 as ‘measured.’ Ideally, the pressure amplitudes of the all five transmitting transducers that contribute to the pressure field at the focal line should constructively sum, since the array is designed such that the distance from each transmitting transducer to the focal line is the same, and the signals should all be in phase. To check if this is true for the as built array, a normalization procedure [17] is used to numerically

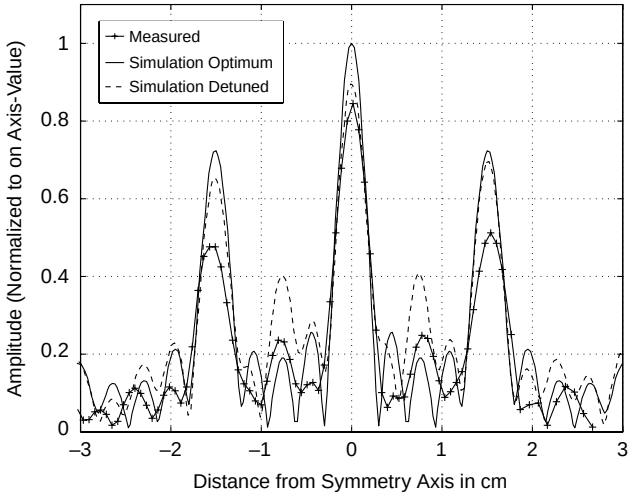

Fig. 6. As built array pressure amplitude (normalized to the maximum reachable) in the y-direction.

calculate this ideal pressure field, which is presented in Fig. 6 as 'simulation optimum.' Comparing both plots—the experimentally measured and simulation optimum—one observes that the height of the main-lobe is 15% lower in the measured result. Furthermore, only one of the first three side-lobes predicted by the simulation is present in the sound pattern of the as built array, and the larger, fourth side-lobe is present, but it is approximately 25% less than numerically predicted.

The discrepancy that causes the greatest change in the shape of the pressure pattern is the actual distance from a single transmitting transducer to the focal line, and a procedure that uses the speed of sound in air is developed to measure this spatial error (and thus the actual radial distance of each transmitting transducer) of the as built array. These 'actual' distances are used in a numerical simulation of the as built array, and presented in Fig. 6 as 'simulation detuned.' The amplitude of the measured main-lobe is only 5% lower than the amplitude in the detuned simulation. Furthermore, the shape of the pressure amplitude corresponds quite well—both plots have two side-lobes present before the major side-lobe at 1.5 cm from the symmetry axis. The pressure amplitude of all the side-lobes is down by 5–15%. This discrepancy could be a result of additional alignment errors, or due to differences in the output level of the individual transmitting transducers. Fig. 6 shows that the as built array does not have exactly the same pressure pattern predicted by the optimized array. Instead, it is shown that the as built array is slightly detuned (on the order of 1 mm). The error is mainly an error in the propagation distance. Therefore, an improved design could include separate transmitting transducer triggers in order to compensate for small differences in propagation distance.

The performance test of the as built array along the x-axis (while all 20 transducers are operating) is characterized by moving the G.R.A.S. microphone along the x-axis on the focal line; this experimentally measured data is compared to the numerically predicted values. A comparison reveals that their shapes match very well and main peaks are at exactly the same locations, and have nearly the same height. A separate phase measurement shows excellent agreement between measured and numerically simulated phase [17].

Finally, the absolute emitted sound pressure level of the as built array is measured as 142.70 dB SPL. But if a different driving amplifier is used to provide a higher input AC voltage, sound pressure levels of up to 150 dB SPL can be achieved with this as built array.

Note that an alternate design for a focused line transducer could be to use a single, continuous source layer on a cylindrical backing plate. This source layer could be a piezoactive film, such as PVDF, or a metallized plastic film driven by electrostatic forces. Such a focussed transducer, using a metallized plastic film with electrostatic drive, was recently developed by [22] for the frequency range 200 kHz–1 MHz. The advantages of a continuous source layer are greater sound pressure level in the focal region and a decrease in the levels of the side lobes.

3.2. Low density polyethylene (LDPE) plate

Consider a plate of low density polyethylene (LDPE) 608×305.5 mm, with a thickness of 41.4 mm. The bulk wave speeds (longitudinal and shear, respectively) $c_L=2095$ m/s and $c_T=707.1$ m/s, plus the Lamé constants $\lambda=3.17$ GPa and $\mu=0.468$ GPa are directly measured in this material [17].

This plate is first used to examine the ultrasonic behavior of the as built array by comparing its performance to a commercial piezoelectric contact transducer (Digital Wave B1025). The input signal in both cases is one cycle of a sine-wave with a frequency of 80 kHz, and the input voltage for the piezoelectric transducer is 100 V, peak-to-peak. The receiving transducer in both cases is a (or another) Digital Wave B1025 transducer. The source–receiver arrangement is through transmission, where the source and the receiver are located on axis (epicenter) on opposite sides of each other through the 41.4 mm thickness. Fig. 7(a) shows the time-domain signal with the as built array source, while Fig. 7(b) shows the time-domain signal from the Digital Wave transducer source. The first motion is observed at 610 μs for the as built array signal, and at 20 μs for the Digital Wave signal (both where triggered at $t=0$). This time difference is due to the additional propagation distance of approximately 205 mm in air for the as built array signal. Note that the amplitude of the ultrasonic signal from the as built array is five-times lower than the one from the contact, piezoelectric transducer. The reason for this decrease is the low efficiency of the air-coupled source, in relative comparison to the piezoelectric source. This inefficiency is expected, and is the reason for developing a focused array. Note that the ultrasonic signal created by the Digital Wave

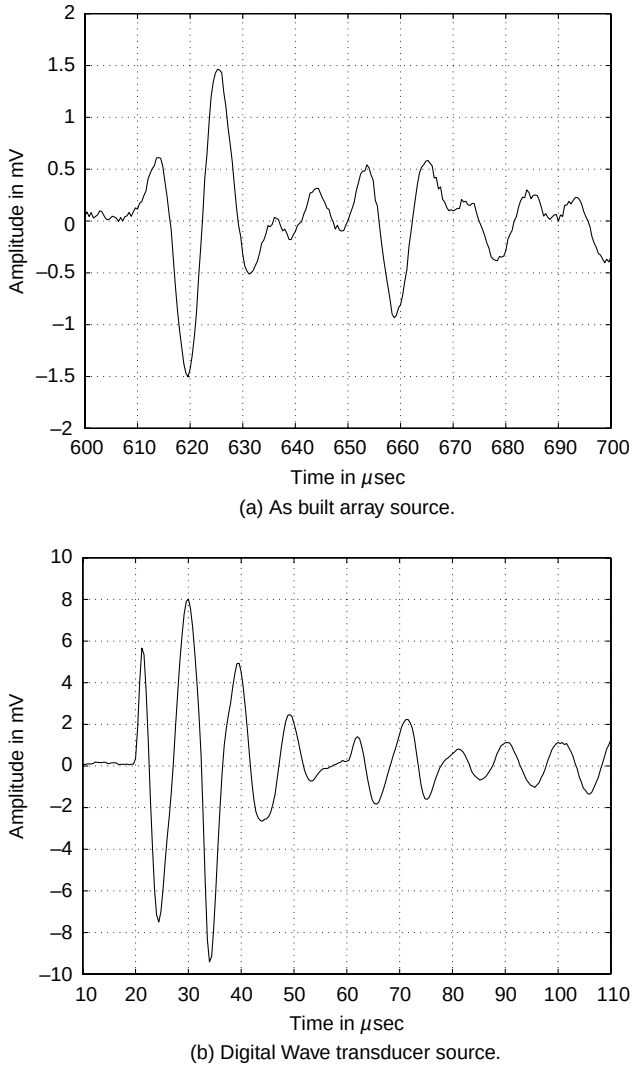

Fig. 7. Comparison of sources—as built array versus a commercial contact piezoelectric transducer.

transducer has three major bursts with an exponentially decreasing amplitude (it rings)—this is representative of the resonant behavior of a piezoelectric source. In contrast, the ultrasonic signal created by the as built array only contains a single burst; there are some smaller (compared to the first burst) bursts arriving between 635 and 655 μs, and the reflection of the first burst arrives at 655 μs. This demonstrates another advantage of the as built array (besides its non-contact nature)—the array can generate well-defined transient signals because the elements of the array have a flat response over the frequency range 20–100 kHz (see Table 1).

As a final step, the as built array is used as a line-source on the LDPE plate, and the resulting ultrasonic signals (through transmission) are detected with a non-contact, laser interferometric receiver [23]. This is a completely non-contact generation/detection system, and is a demonstration of the viability of a non-contact, ultrasonic scanning system for civil infrastructure. The LDPE plate can be treated as a semi-infinite half-space for short times, before reflections corrupt the experimentally measured signal. An analytical solution for a perpendicular line-load on a semi-infinite half-space (Lamb's problem) is available [24], so it is possible to validate the robustness and accuracy of the as built array by comparing measured and numerically simulated ultrasonic signals in the LDPE plate.

Two bursts of a sine-wave with a frequency of 80 kHz are transmitted by the as built array, and the laser interferometer is used as a detector—the laser interferometer measures absolute particle velocity (out-of-plane) with high fidelity [23]. The source–receiver arrangement is through transmission, where the source and the receiver are located on opposite sides of each other through the 41.4 mm thickness. The out-of-plane particle velocity is measured at four locations—epicenter (on the symmetry axis), and at distances of 20, 30, and 40 mm from the symmetry axis. Figs. 8–11 show the particle velocity measured at these four locations—the measured signals represent 350 time averages, and have been low-pass filtered at 120 kHz. These experimentally measured time-domain signals are compared to their respective numerically simulated counterparts, which are developed following [24], and are numerically differentiated to match the measured results, changing particle displacement to particle velocity. It is important to note that the numerically simulated results are valid for a semi-infinite half-space, with no reflections from a 'bottom surface.' This is in contrast to the experimental measurements, where the LDPE specimen has a finite thickness of 41.4 mm, and the incident waves will be reflected from this boundary. A comparison between the numerically simulated and experimentally measured results is only valid in a finite time window—for the times before the reflected waves from the lower boundary have reached the measurement position. This time window (when no reflected signal is present) is calculated and Figs. 8–11 identify this region (shaded) as the 'trusted region.'

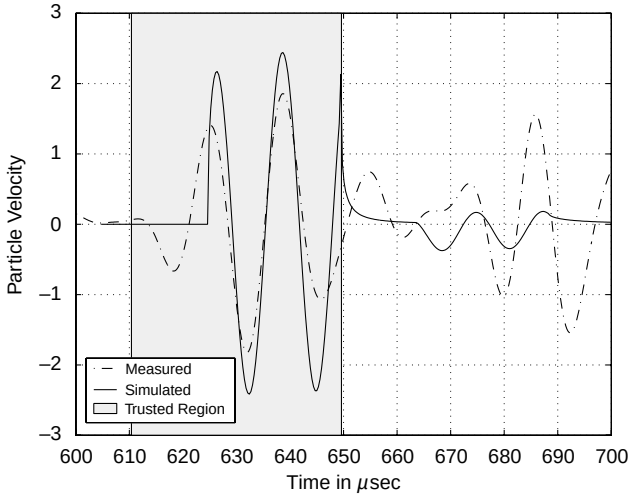

Fig. 8. Particle velocity (arbitrary units) at $y=0$ mm from symmetry axis (epicenter).

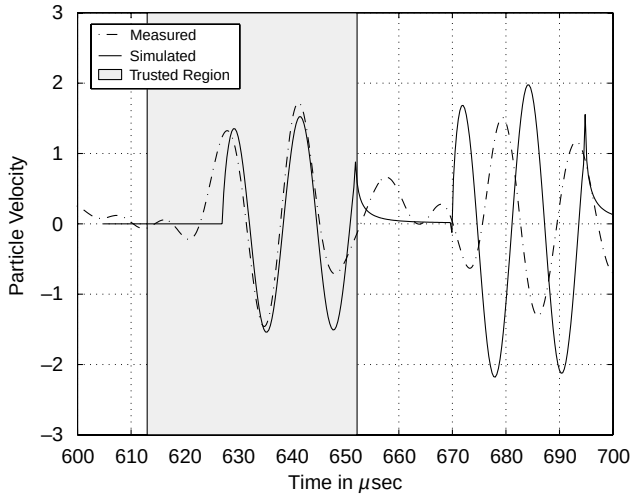

Fig. 9. Particle velocity (arbitrary units) at $y=20$ mm from symmetry axis.

Note that the amplitudes of the numerically simulated results are normalized to the measurement at $y=20$ mm—this normalization ratio is maintained for all the other simulations, and allows for consistent comparisons.

The measured signal in Fig. 8 (and to a lesser extent, Fig. 9) has an initial negative (downwards) component, before the arrival time predicted by the numerical simulation. This (physically impossible, non-causal) effect is due to the transmitting transducers in the as built array—there is an initial pulse when the transmitting transducers are subjected to the input AC signal. The steep slope at the beginning of all the numerically simulated results is a by-product of the numerical differentiation, and it should be of the same steepness as the slope after one period of the sine signal.

Taking these effects into account, there is excellent agreement between the numerically simulated and experimentally measured signals in the trusted regions. There is a small difference in the epicenter measurements

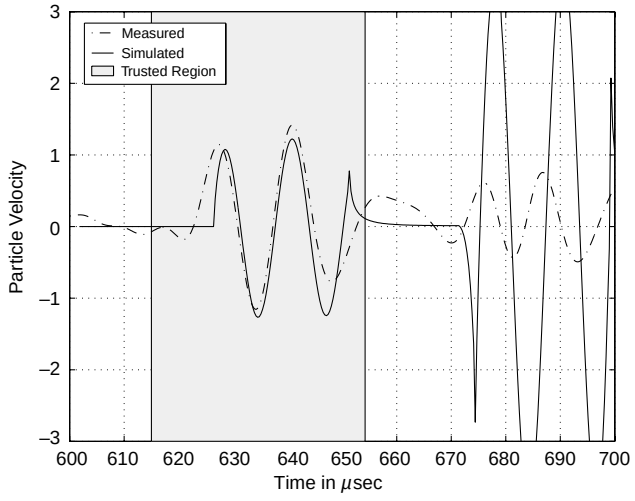

Fig. 10. Particle velocity (arbitrary units) at $y=30$ mm from symmetry axis.

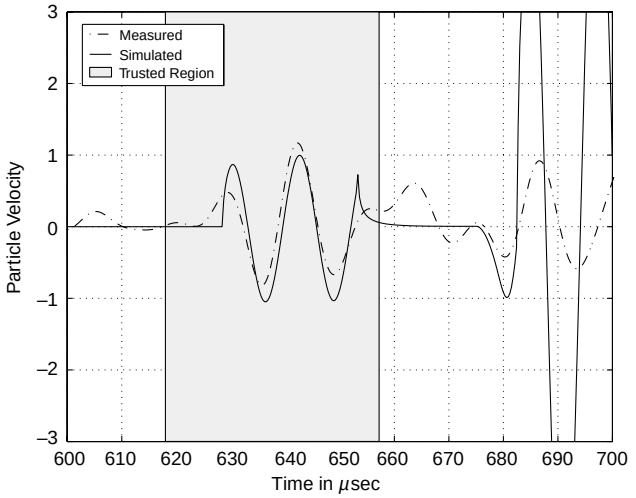

Fig. 11. Particle velocity (arbitrary units) at $y=40$ mm from symmetry axis.

(Fig. 8)—the numerically predicted amplitudes are 20% higher than the experimentally measured values in this plot, but the overall shapes are in good agreement. This discrepancy could be due to small errors in positioning the receiving heterodyne-interferometer (there is a positioning error on the order of 3 mm), since the epicenter predictions are very position sensitive.

Overall, this set of measurements shows that the experimentally measured signals in the LDPE plate match the numerically simulated results using the model of a half-space subjected to a line-load (Lamb's problem). It can then be concluded that the as built array generates a pressure field that is very close to a line-source—this is a primary aim of the original design.

It is of interest to compare the present study with the work of [15]. In both cases non-contact NDE systems were developed using a combination of lasers and air-coupled transducers. However, the system developed in this study has advantages for NDE of civil structures in the frequency range 50–100 kHz. In this frequency range elastic waves are more efficiently generated with a focused air-coupled transducer than with a high-power laser. Also, detection of the elastic waves with a laser Doppler vibrometer allows measurement of both in-plane and out-of-plane particle velocity components [7], whilst detection with an air-coupled transducer is related only to the out-of-plane velocity component.

4. Conclusion

This research develops, builds and characterizes a two dimensional, air-coupled array for the non-contact generation of ultrasound. The design process consists of the development of a numerical model that simulates the pressure field emitted by an array of electrostatic transducers. This numerical simulation drives the design process,

with complementary experimental measurements used to verify the accuracy and robustness of these predictions. The numerical model is used to design the final array—the overall design objective is to position 20 electrostatic transducers in such a way that the signal amplitude at the focal line of the array is maximized. A sensitivity study is performed to identify the most critical parameters that change the predicted behavior of the array. It is concluded that changes in the spatial position of the transmitting transducers (0.5 mm at frequencies around 100 kHz) have a significant effect on the signal at the focal line, especially if a transmitting transducer is moved radially towards the focal line. With this knowledge, the array is built; the total material costs of the array, including transducers, is on the order of $500.

A set of experiments is performed to quantify the behavior of the as built array. It is determined that the absolute emitted sound pressure level (in air) of the array is 142.70 dB SPL, and it might be possible to achieve pressure levels of up to 150 dB SPL.

Experiments are performed in low density polyethylene components to quantify the ultrasonic signal characteristics generated by the as built array, and the source behavior of the array is compared to that of a piezoelectric contact transducer. These measurements show that the amplitude of the ultrasonic waves generated with the air-coupled array is on the order of five times lower than the signal generated by a piezoelectric, contact transducer. In addition, the transient behavior of the array is less resonant than the contact transducer. The last set of experiments shows that, by comparing the measured data to the numerical simulation of a half-space subjected to a line-load, the array acts like a line-source, which is an aim of the design process. There is excellent agreement between the experimental and numerical representations, which confirms the efficiency of the as built array, and confirms the possibility of developing a completely non-contact, scanning ultrasonic system in the 50–100 kHz range.

Acknowledgements

A The Deutscher Akademischer Austausch Dienst (DAAD) provided partial support to Frank Blum. The National Science Foundation (NSF) provided partial support to Laurence Jacobs through Grant No. CMS-0201283.

References

[1] Pla-Rucki GF, Eberhard MO. Imaging of reinforced concrete: state-of-the art review. J Infrastruct Syst 1995;1(2):134–41.

[2] Komlos K, Popovics S, Nürnbergrová T, Babál B, Popovics JS. Ultrasonic pulse velocity test of concrete properties as specified in various standards. Cem Concr Compos 1996;18(5):357–64.

[3] Martin J, Broughton KJ, Giannopolous A, Hardy MSA, Forbe MC. Ultrasonic tomography of grouted duct post-tensioned reinforced concrete bridge beams. NDT&E Int 2001;34(2):107–13.

[4] Krause M, Mielentz F, Milman B, Müller W, Schmitz V, Wiggenhauser H. Ultrasonic imaging of concrete members using an array system. NDT&E Int 2001;34(6):403–8.

[5] Landis EN, Shah SP. Frequency-dependent stress wave attenuation in cement-based materials. J Eng Mech 1995;121(6):737–43.

[6] Kil H-G, Jarzynski J, Berthelot Y. Wave decomposition of the vibrations of a cylindrical shell with an automated scanning laser vibrometer. J Acoust Soc Am 1998;104(6):3161–8.

[7] Stolzenburg JC, Doane JW, Jarzynski J, Jacobs LJ. Near field inversion method to measure the material properties of a layer. NDT&E Int 2003;36(7):523–33.

[8] Scruby CB, Drain LE. In: Laser ultrasonics: techniques and applications. Bristol: Adam Hilger; 1990.

[9] Owino JO, Jacobs LJ. Attenuation measurements in cement-based materials using laser ultrasonics. J Eng Mech 1999;125(6): 637–47.

[10] Martínez O, Akhnak M, Ullate LG, de Espinosa FM. A small 2d ultrasonic array for ndt application. NDT&E Int 2003;36(1):57–63.

[11] Mendelsohn Y, Wiener-Avnear E. Simulations of circular 2d phase-array ultrasonic imaging transducers. Ultrasonics 2002;39(9):657–66.

[12] Holland SD, Teles SV, Chimenti DE. Air-coupled, focused ultrasonic dispersion spectrum reconstruction in plates. J Acoust Soc Am 2004; 115(6):2866–72.

[13] McNamara J, di Scalea FL. Air coupled ultrasonic testing of railroad rails. Mater Eval 2002;60(12):1431–7.

[14] Grandia WA, Fortunko CM. Nde application of air-coupled ultrasonic transducers. Proceedings of the IEEE ultrasonic symposium 1995 p. 697–709.

[15] Hutchins D, Wright W, Hayward G, Gachagan A. Air-coupled piezoelectric detection of laser-generated ultrasound. IEEE Trans UFFC 1994;41:796–805.

[16] Kinsler LE, Frey AR, Coppens AB, Sanders JV. Fundamentals of acoustics. 3rd ed. New York: Wiley; 1982.

[17] Blum F. A focused, two dimensional, air-coupled ultrasonic array for non-contact generation. Master's thesis. Engineering Science and Mechanics, Georgia Institute of Technology, Atlanta, GA; 2003.

[18] Bass HE, Sutherland LC, Piercy J, Evans L. In: Mason WP, Thurston R, editors. Absorption of sound by the atmosphere. Pysical acoustics, vol. XVII. Academic Press, Inc.; 1984. p. 145–232.

[19] Group POC. Polaroid ultrasonic ranging system handbook application notes/technical papers.

[20] Goldberg DE. Genetic algorithms in search, optimization, and machine learning. Learning: Addison-Wesley Pub. Co.; 1989.

[21] Blum F. Ein beitrag zur entwicklung einer innovativen virtuellen optimierungsmaschine für die kraftwerkstechnik, Studienarbeit, IVD-Universität Stuttgart, in German; 2002.

[22] Robertson T, Hutchins D, Billson D. An air-coupled line-focused capacitive ultrasonic transducer. Proceedings of the IEEE ultrasonic sympomsium 2000 p. 1061–1064.

[23] Bruttomesso DA, Jacobs LJ, Costley RD. Development of an interferometer for acoustic emission testing. J Eng Mech 1993; 119(11):2303–16.

[24] Miklowitz J. The theory of elastic waves and waveguides. Amsterdam: North-Holland Pub. Co; 1978.